Evaluation of a Primary-Side Parameters-Agnostic Power Regulation Method on Different WPT Topologies

This is the author's version of the article that has been presented at IEEE MWSCAS2023
The editorial version of the paper is available at http://dx.doi.org/10.1109/MWSCAS57524.2023.10405900

Evaluation of a Primary-side Parameters-agnostic Power Regulation Method on Different WPT Topologies

Andrea Celentano*, Carmine Paolino*,‖, Fabio Pareschi*,†, Riccardo Rovatti†,‡, Gianluca Setti§
* DET – Politecnico of Torino, corso Duca degli Abruzzi 24, 10129 Torino, Italy.
email:{andrea.celentano, fabio.pareschi}@polito.it
‖ Nanolab, Advanced Technology Laboratory, ECE – Tufts University, 02155 Medford, MA, USA
email:carmine.paolino@tufts.edu
† ARCES – University of Bologna, via Toffano 2/2, 40125 Bologna, Italy.
‡ DEI – University of Bologna, viale Risorgimento 2, 40136 Bologna, Italy. email: riccardo.rovatti@unibo.it
§ CEMSE, King Abdullah University of Science and Technology (KAUST), Saudi Arabia. e-mail: gianluca.setti@kaust.edu.sa

***Abstract*—A recent paper has introduced a primary-side control methodology for Wireless Power Transfer (WPT) links, capable of delivering, by only sensing quantities available at the primary side (i.e., the power transmitter), the optimal power level to the load without compromising the system efficiency. Indeed, this technique has been validated only on an ad-hoc WPT system relying on an isolated class-E DC-DC power converter based on inductive coupling. In this paper we provide results, through SPICE simulations, by applying the proposed approach to different state-of-art WPT systems, either inductively or capacitively coupled, in order to improve the generality of the adopted control methodology and to extend the validity of the method beyond the circuit topology considered in the original paper.**

I. Introduction

Wireless Power Transfer (WPT) is an emerging technique that aims to replace standard wired power supplies in an increasing amount of applications. Limiting the scope to near field transfer only, two basic WPT methodologies can be identified, namely inductive [1], [2] and capacitive coupling [3], [4].

Design methodologies for WPT systems can either focus separately on the power transmitter and power receiver side [5]–[8] or consider these two blocks simply as part of an isolated DC-DC converter characterized by a low coupling factor k [3], [9]–[12].

Whatever the adopted design methodology, a robust WPT system should deal with load variations, the load being the time-varying electronics that must be fed by the source at the primary side, as well as misalignment, variable distance, and medium between transmitter and receiver that turn the parameter k into an unknown variable. In order to improve the system robustness and guarantee Maximum Efficiency Transfer (MET) [13], [14] to the load, information about the received power is conventionally sent back to the transmitter via the same link (back telemetry) [7], [15], [16]. However, the complexity and power consumption of the receiver unit increase, resulting in limited efficiency and data rates. Therefore, links that adjust their operation by sensing the performance exclusively at the transmitter side (without the need for feedback) are desirable.

The foundation of this work was laid in [17] and later expanded in [13], where both theoretical and experimental investigations were conducted on the existence and identification of a MET point when a regulator is added at the secondary side. Indeed this leads to a corner in the input–voltage characteristic of the converter and allows the primary-side-only control without the need for additional data links or complex circuitry at the secondary side. Moreover, the technique is robust even against the variation of both the coupling coefficient and load. Here, we expand the observations in [13], where the solution was proven to work on a specific circuit only, by identifying the presence of the MET point in recently proposed, state-of-the-art WPT systems.

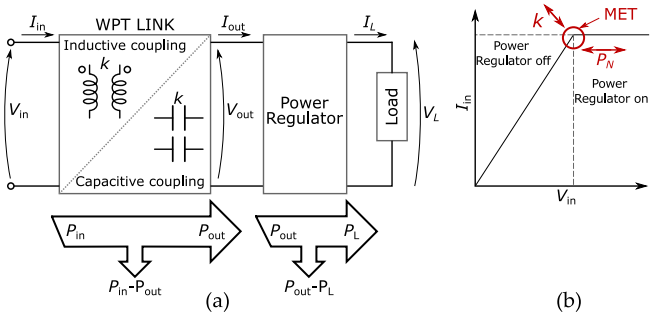

Fig. 1. (a) Schematic diagram of a WPT system including a power regulator between the DC-DC and the load. (b) $I_{\rm in} - V_{\rm in}$ curve that clearly shows a corner point when the MET condition is encountered.

This paper is organized as follows. In Section II we briefly overview the MET methodology shown in [13]. In Section III we apply the methodology to recent WPT systems available in the literature. Finally we draw the conclusion.

II. Review of the Methodology

In this section we briefly review the methodology for the MET point identification, fully detailed in [13]. Accordingly, it is required the addition of a power regulator between the WPT link and the load, as depicted in Figure 1(a).

For the sake of simplicity, the WPT system is considered as a voltage-controlled black box whose output power $P_{\rm out}$ depends on the input voltage $V_{\rm in}$ and on the coupling factor k. Then, the WPT link is connected to the power regulator that dissipates the excess power and delivers the right power P_L to the load. P_L can also be time-varying (i.e., the absorbed *nominal* power, P_N, can change over time). As shown in Figure 1(a), in order to set the load power P_L to the desired value P_N it is required that the regulator is aware of P_N and that $P_{\rm out} > P_N$. The regulator dissipates $P_{\rm out} - P_N$, so that $P_L = P_N$. However, the MET condition is not encountered unless the the power regulator is only marginally on, dissipating a negligible amount of power. In this case, $P_{\rm out} \approx P_N$, and the MET condition is ensured. In practice, the MET condition can be achieved by setting $V_{\rm in}$ to the value resulting in $P_{\rm out} \approx P_N$. We denote this level as $V_{\rm in}^{(opt.)}$.

In [13], it has been demonstrated that the value of $V_{\rm in}^{(opt.)}$ can be easily identified by looking at the current-to-voltage characteristic from the WPT-link primary side, only. The $I_{\rm in}$–$V_{\rm in}$ curve shows a *corner point*, i.e., a *discontinuity* in its derivative as simplified in Figure 1(b), that corresponds exactly to the MET point, leading to its

This is the author's version of the article that has been presented at IEEE MWSCAS2023
The editorial version of the paper is available at http://dx.doi.org/10.1109/MWSCAS57524.2023.10405900

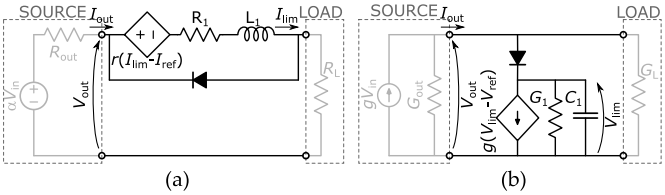

Fig. 2. (a) Schematic of the circuit used as series power regulator (current limiter). (b) Schematic of the circuit used as shunt power regulator (voltage limiter).

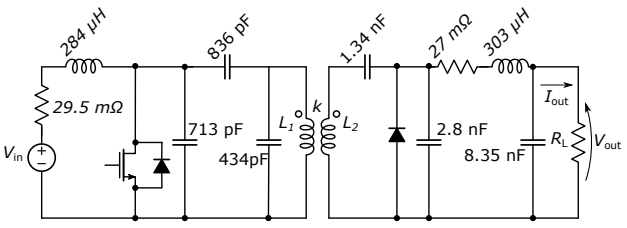

Fig. 3. Schematic of the Class-E^2 DC-DC converter based on inductive coupling taken from [11].

correct identification with no knowledge of k, P_N or even the system model. Once the MET point has been found, it can also be tracked to compensate for possible variations in k and P_N and therefore ensure the right power to the load while achieving minimum power dissipation by the regulator.

According to [13], in which two types of power regulators (i.e., a series power regulator and a shunt one) are considered, the only requirement to be satisfied for an accurate MET identification concerns the output resistance (or conductance) of the WPT link with respect to the load resistance (or conductance) computed at the nominal operating point. This is paramount since the MET point can be identified if the corner point in the $I_{\rm in}$–$V_{\rm in}$ curve can be easily observed, i.e.

$$R_{\rm out} \ll \frac{P_N}{I_N^2}\,, \tag{1}$$

for a series power regulator. While:

$$G_{\rm out} \ll \frac{P_N}{V_N^2}. \tag{2}$$

for a parallel power regulator. The derivation of the above expressions is based on the comparison of the derivatives of the $I_{\rm in}$–$V_{\rm in}$ curve on both sides of the MET point and is included in full in [13].

III. Application to state-of-the-art WPT systems

In this section, three recently proposed WPT systems [3], [11], [12] are analyzed by means of SPICE simulations. The analysed topologies are significantly different from one another, and also from the topology of the reference methodology [13], [17] so as to highlight the versatility of the proposed MET identification method for the robust regulation of the load operating conditions against coupling factor and load variations. We consider each design exactly as proposed in the corresponding reference publication, with the addition of either a current limiter or a voltage limiter as power regulator, depending on the circuit characteristics according to (1) and (2).

The schematic used for the current limiter is shown in Figure 2(a), assuming the simple case of a resistive load R_L and a Thevenin circuit equivalent source. The circuit is based on a transresistance difference amplifier with gain r, operating in negative feedback. Assuming $R_{\rm out} \ll R_L \ll R_1$, the open-loop gain is $A = I_{\rm lim}/(I_{\rm lim} - I_{\rm ref}) = r/R_1$ ($I_{\rm ref}$ being the reference current for the power regulator), and the feedback loop sets $I_{\rm lim} \approx AI_{\rm ref}/(1+A)$, which approximates $I_{\rm ref}$ for sufficiently large values of A. When the (ideal) diode is off, we get $I_L = I_{\rm lim}$, whereas for $I_L < I_{\rm ref}$ the diode turns on, thus disabling the current limiter. The inductance L_1 is added to limit the bandwidth of the current limiter, as it adds a pole at a frequency of approximately $r/(2\pi L_1)$.

The schematic used for the voltage limiter in the simple case of a conductance load G_L and a Norton equivalent circuit source is depicted in Figure 2(b) and it is based on a transconductance difference amplifier with gain g. Assuming $G_{\rm out} \ll G_L \ll G_1$, the open-loop gain is $A = V_{\rm lim}/(V_{\rm lim} - V_{\rm ref}) = g/G_1$ ($V_{\rm ref}$ being the reference voltage for the power regulator) and $V_{\rm lim} \approx AV_{\rm ref}/(1+A)$ that approximates $V_{\rm ref}$ for sufficiently large values of A. When the ideal diode is on we have $V_L \approx V_{\rm lim}$, whereas for $V_L < V_{\rm ref}$ the diode turns off thus disabling the limiter. The role of C_1 is to limit the bandwidth by adding a pole at approximately $g/(2\pi C_1)$.

In the following, we will set $A = 100$ and limit the bandwidth of the limiter to $1/10$ of the WPT switching frequency.

A. Classic Inductive Class-E ^{2} converter topology

The class-E^2 converter in Figure 3 is taken from [11], and its design relies on the classic approach known as *sinusoidal approximation*. This method considers the AC component of all waveforms as a single tone at the switching frequency f_s. The rectifier circuit (at the secondary side of the transformer) can then be approximated as an equivalent impedance and, therefore the class-E inverter (at the primary side of the transformer) can be designed as a single-tone power amplifier loaded by the reflected impedance of the rectifier. Of course, for the sinusoidal approximation to be effective, additional filtering elements tuned at the first harmonic are required, so that the actual waveforms resemble sinusoids.

Specs and Nominal Design–The system in [11] is designed for $P_{\rm out} = 5\,{\rm W}$, input voltage $V_{\rm in} = 20\,{\rm V}$ and a resistive load $R_L = 50\,\Omega$ (so $I_{\rm out} = 316\,{\rm mA}$), and operates at the frequency $f_s = 1\,{\rm MHz}$. Additionally, the coupled coils have a quality factor $Q \approx 170$ at the nominal frequency and the coupling coefficient is specified as $k = 0.1$.

The active devices were simulated using the available SPICE models of the actual components used in [11], i.e. a SUD06N10-225L by Vishay as the main MOS, switching with a duty cycle $D = 0.5$, and a STPS5H100B Schottky barrier diode by STMicroelectronics as the rectifying diode. All other components have been either assumed ideal, or their parasitics have been explicitly shown in Figure 3. Component values are directly shown in the figure.

Output Characteristic–The $V_{\rm out}$–$I_{\rm out}$ characteristic of this DC-DC converter can be seen in Figure 4(a), and has been obtained by sweeping the resistive load at the nominal input voltage $V_{\rm in} = 20\,{\rm V}$ and variations of $\pm 25\%$ around it.

The plot shows a real voltage source behaviour, hence regulation can be obtained by adding a series limiter to the secondary side. To be consistent with [11], we set $I_N = 316\,{\rm mA}$. Furthermore, (1) is satisfied, as can be seen from Figure 4(b) that compares the observed value of $R_{\rm out}$ from Figure 4(a) with the $50\,\Omega$ resistive load.

Input Characteristic and MET point–For this system we have considered three different nominal power levels $P_N = 3\,{\rm W}$, $P_N = 4\,{\rm W}$ and $P_N = 5\,{\rm W}$, and three coupling coefficient values $k = 0.08$, $k = 0.1$, $k = 0.2$.[1] Only the case of a resistive load $R_L = P_N/I_N^2$

[1]Note that, the perturbations of both the coupling factor and of the nominal power are limited since a larger variation would lead to unacceptable stress on the MOS.

This is the author's version of the article that has been presented at IEEE MWSCAS2023
The editorial version of the paper is available at http://dx.doi.org/10.1109/MWSCAS57524.2023.10405900

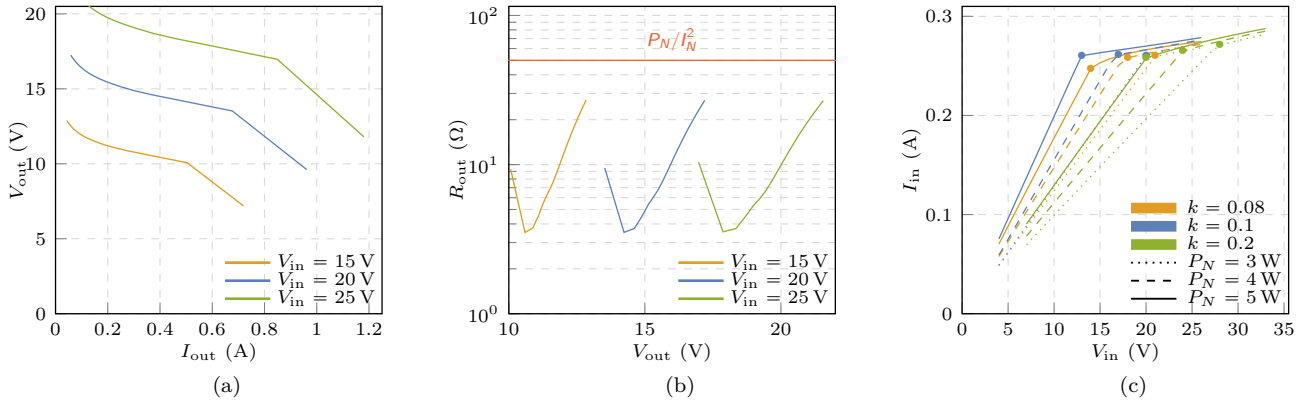

Fig. 4. Characteristics of the classical class-E^2 DC-DC converter based on inductive coupling: (a) output curves of the converter for three different input voltages from which the voltage source behaviour becomes clear. (b) output resistance of the converter compared to that of the nominal load in order to justify the use of a current limiter. (c) I–V characteristics observed at the primary side of the DC-DC isolated converter for three different coupling factor values $k = 0.08$, $k = 0.1$, $k = 0.2$ and three different nominal power levels $P_N = 3\,\mathrm{W}$, $P_N = 4\,\mathrm{W}$, $P_N = 5\,\mathrm{W}$. The bullet points indicate the MET point identified according to the algorithm proposed in [13].

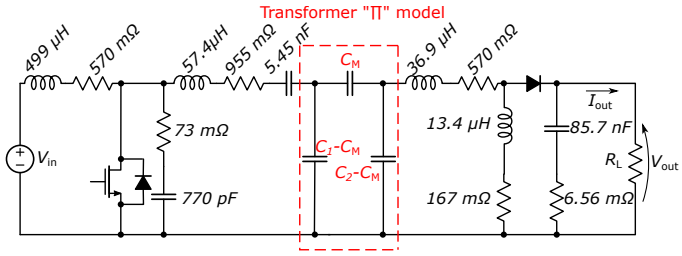

Fig. 5. Schematic of the class-E^2 DC-DC converter based on capacitive coupling taken from [3].

has been considered.

The I_{in}–V_{in} characteristic has been plotted in Figure 4(c), and shows the expected behaviour. Irrespective of the nominal power and of the coupling coefficient, the system shows a discontinuity in the derivative of the I_{in}–V_{in} curve. Therefore, this point, which represents the MET point, can be easily identified even without knowledge of k and P_N.

B. Capacitive Class-E^2 Converter Topology

In [3], a WPT system based on capacitive coupling and designed according to the aforementioned sinusoidal approximation, is proposed. Its schematic is depicted in Figure 5, highlighting the π capacitive transformer model. Capacitances C_1 and C_2 represent the total primary and secondary capacitance, respectively. The mutual capacitance is $C_M = k\sqrt{C_1 C_2}$, with k the coupling coefficient, as in the inductive case. Their value is $C_1 = C_2 = 559\,\mathrm{pF}$ and $C_M = 55.9\,\mathrm{pF}$.

Specs and Nominal Design–The specifications are: $f_s = 1\,\mathrm{MHz}$, $V_{out} = 15\,\mathrm{V}$, $P_{out} = 2\,\mathrm{W}$ at $D = 0.5$[2] and $k = 0.1$. Furthermore, $R_L = 111\,\Omega$ and the nominal behaviour is achieved for $V_{in} = 11\,\mathrm{V}$.

For the MOS transistor and the diode we have used the available SPICE model of the IRF510 and RB160VAM-60, respectively. For all reactive components, a simple model with parasitic series resistance has been considered, as explicitly shown in Figure 3.

Output Characteristic–The circuit, according to the I_{out}–V_{out} characteristic of Figure 6(a), computed for the nominal input voltage $V_{in} = 11\,\mathrm{V}$ and its ±25% variations $V_{in} = 8.25\,\mathrm{V}$ and $V_{in} = 13.75\,\mathrm{V}$, has the same behavior as a real current source. Therefore, the MET identification can be performed by adding a shunt regulator (we set $V_N = 15\,\mathrm{V}$) and by satisfying (2). To this purpose, we have compared in Figure 6(b) the observed output conductance of the DC-DC converter with the load conductance value $P_N/V_N^2 = 9\,\mathrm{mS}$ at $P_N = 2\,\mathrm{W}$. It is clear from the figure that (2) is satisfied.

Input Characteristic and MET point–The I_{in}–V_{in} characteristic for this system has been plotted in Figure 6(c). We have considered three nominal power levels $P_N = 1.5\,\mathrm{W}$, $P_N = 2\,\mathrm{W}$ and $P_N = 2.5\,\mathrm{W}$, and three nominal coupling coefficient $k = 0.06$, $k = 0.1$ and $k = 0.2$. Only the conductive load case has been taken into account.

Again, irrespective of the nominal power, the system behaves in a similar way in all cases by showing a discontinuity in the derivative of the I_{in}–V_{in} curve. Therefore this point, which represents the MET point, can be easily identified independently of k and P_N.

C. Inductive Class-E-DE Circuit Topology

In [12], one more WPT system based on inductive coupling is proposed. The converter schematic is depicted in Figure 7 and it is made of a class-E inverter and a class-DE rectifier.

Specs and Nominal Design–The system in [12] is designed for $P_{out} = 10\,\mathrm{W}$, input voltage $V_{in} = 24\,\mathrm{V}$ and a resistive load $R_L = 50\,\Omega$ (so $I_{out} = 447\,\mathrm{mA}$)[3], and operates at the frequency $f_s = 1\,\mathrm{MHz}$. Additionally, the coupled coils L_1 and L_2 have a quality factor Q at the nominal frequency equals to 165 and 170, respectively, and the coupling coefficient is specified to be $k = 0.056$.

The active devices were simulated using the available SPICE models of the actual components used in [12], i.e. a IRFS4410 by International Rectifier as the main MOS, switching with a duty cycle $D = 0.5$, and a STPS5H100B Schottky barrier diode by STMicroelectronics as diodes at the rectifier side. All other components have been either assumed ideal, or their parasitics have been explicitly shown in Figure 3. Component values are directly shown in the figure.

Output Characteristic–The circuit, according to the V_{out}–I_{out} characteristic of Figure 8(a), computed for the three input voltages $V_{in} = 18\,\mathrm{V}$ and $V_{in} = 22\,\mathrm{V}$ and $V_{in} = 24\,\mathrm{V}$, shows the behavior of a real voltage source. Therefore, the MET identification can be performed by adding a current limiter and by setting $I_N = 360\,\mathrm{mA}$

[2]In [3], the duty cycle is declared to be $D = 0.6$. However, according to the measurements shown by the authors, it is clear that $D = 0.5$.

[3]Spice simulations by using available SPICE models of the adopted components show $I_{out} = 360\,\mathrm{mA}$ and therefore $P_{out} = 6.5\,\mathrm{W}$.

This is the author's version of the article that has been presented at IEEE MWSCAS2023
The editorial version of the paper is available at http://dx.doi.org/10.1109/MWSCAS57524.2023.10405900

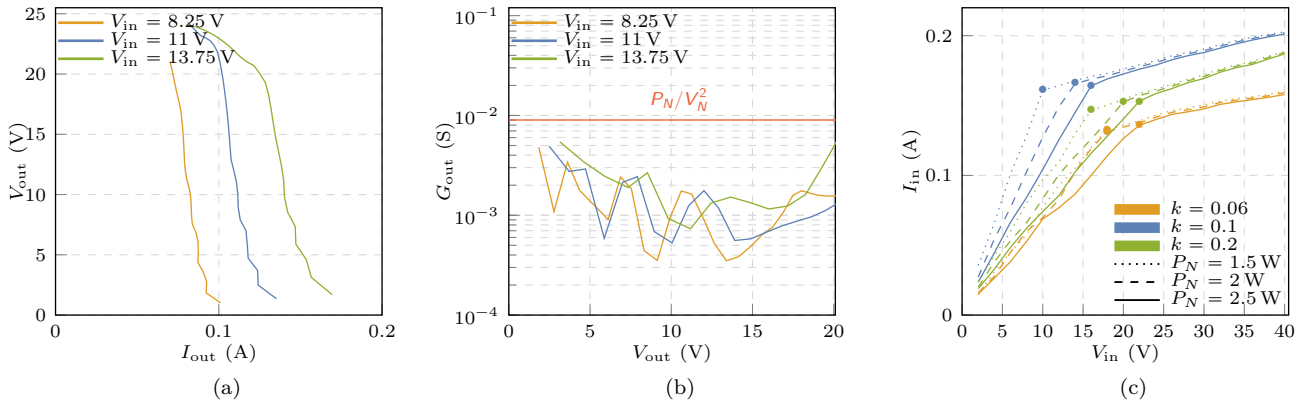

Fig. 6. Characteristics of the classical class-E^2 DC-DC converter based on capacitive coupling: (a) output curves of the converter for three different input voltages from which the current source behaviour becomes clear; (b) output conductance of the converter compared to that of the nominal load in order to justify the use of a shunt regulator; (c) characteristics observed at the primary side of the DC-DC isolated converter for three different coupling factor values $k = 0.06$, $k = 0.1$, $k = 0.2$ and three different nominal power levels $P_N = 1.5\,\mathrm{W}$, $P_N = 2\,\mathrm{W}$, $P_N = 2.5\,\mathrm{W}$. The bullet points indicate the MET point identified according to the algorithm proposed in [13].

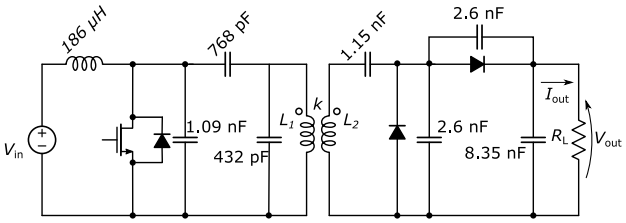

Fig. 7. Schematic of the class-E-DE converter based on inductive coupling taken from [12]

according to the nominal SPICE simulations. Furthermore, (1) is satisfied as can be seen from Figure 8(b) that compares the observed value of R_{out} with the $50\,\Omega$ resistive load.

Input Characteristic and MET point–For this system we have considered three different nominal power levels $P_N = 6\,\mathrm{W}$, $P_N = 6.5\,\mathrm{W}$ and $P_N = 7\,\mathrm{W}$, and three coupling coefficient values $k = 0.05$, $k = 0.06$, $k = 0.07$. Only the case of a resistive load $R_L = P_N/I_N^2$ has been considered.

The I_{in}–V_{in} characteristic has been plotted in Figure 8(c), and shows the expected behaviour. Irrespective of the nominal power and of the coupling coefficient, the system shows a discontinuity in the derivative of the I_{in}–V_{in} curve. Therefore, this point, which represents the MET point, can be easily identified even without any knowledge of k and P_N.

IV. Conclusion

This paper validated a Maximum Efficiency Transfer identification methodology to regulate load power without any information from the receiver part (such as, for example, in the case of active telemetry) or a precise system model. In all the setups being evaluated, a corner point (i.e., a discontinuity in the derivative) in the current–voltage characteristic at the transmitter side, could be observed, notwithstanding both coupling factor and load variations. The addition of either a current limiter, or a shunt regulator, at the receiver side was based on the ratio of the converter output resistance versus the load one. The robustness of the technique in SPICE simulations of recently proposed state-of-the-art WPT systems (i.e, a classic inductive class-E^2, a classic capacitive class-E^2, and an inductive class-E-DE topology) proved the validity of the methodology.

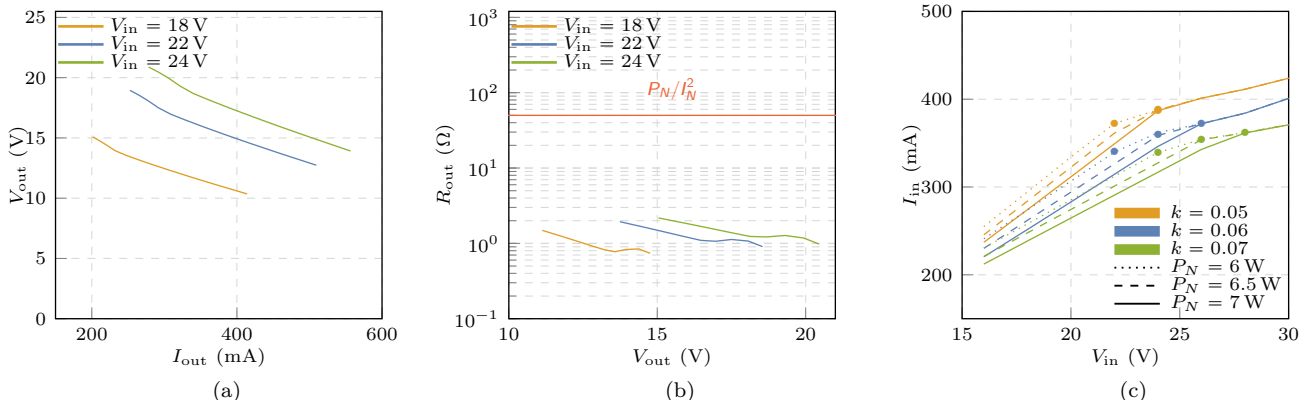

Fig. 8. Characteristic of the class-E-DE DC-DC converter based on inductive coupling: (a) output curves of the converter for three different input voltages from which the voltage source behaviour becomes clear; (b) output resistance of the converter compared to that of the nominal load in order to justify the use of a current limiter; (c) characteristics observed at the primary side of the DC-DC isolated converter for three different coupling factor values $k = 0.05$, $k = 0.06$, $k = 0.07$ and three different nominal power levels $P_N = 6\,\mathrm{W}$, $P_N = 6.5\,\mathrm{W}$, $P_N = 7\,\mathrm{W}$. The bullet points indicate the MET point identified according to the algorithm proposed in [13].

REFERENCES

[1] K. van Schuylenbergh and R. Puers, *Inductive powering: Basic theory and application to biomedical systems*, ser. Analog circuits and signal processing. Dordrecht: Springer, 2009.

[2] T. Sun, X. Xie, and Z. Wang, *Wireless power transfer for medical microsystems*. New York: Springer, 2013.

[3] H. Ueda and H. Koizumi, "Class-e2 DC-DC converter with basic class-e inverter and class-e ZCS rectifier for capacitive power transfer," *IEEE Trans. Circuits Syst. II Express Briefs*, vol. 67, no. 5, pp. 941–945, May 2020. doi: 10.1109/TCSII.2020.2981131

[4] E. Abramov, I. Zeltser, M. M. Peretz, and M. M. Peretz, "A Network-Based Approach for Modeling Resonant Capacitive Wireless Power Transfer Systems," *CPSS Transactions on Power Electronics and Applications*, vol. 4, no. 1, pp. 19–29, Mar. 2019. doi: 10.24295/CPSSTPEA.2019.00003

[5] M. Schormans, V. Valente, and A. Demosthenous, "Practical Inductive Link Design for Biomedical Wireless Power Transfer: A Tutorial," *IEEE Trans. Biomed. Circuits Syst.*, vol. 12, no. 5, pp. 1112–1130, Oct. 2018. doi: 10.1109/TBCAS.2018.2846020

[6] Hao Jiang *et al.*, "A Low-Frequency Versatile Wireless Power Transfer Technology for Biomedical Implants," *IEEE Trans. Biomed. Circuits Syst.*, vol. 7, no. 4, pp. 526–535, Aug. 2013. doi: 10.1109/TBCAS.2012.2220763

[7] Y. Park *et al.*, "A Wireless Power and Data Transfer IC for Neural Prostheses Using a Single Inductive Link With Frequency-Splitting Characteristic," *IEEE Transactions on Biomedical Circuits and Systems*, vol. 15, no. 6, pp. 1306–1319, Dec. 2021. doi: 10.1109/TBCAS.2021.3135843

[8] G. L. Barbruni, P. M. Ros, D. Demarchi, S. Carrara, and D. Ghezzi, "Miniaturised Wireless Power Transfer Systems for Neurostimulation: A Review," *IEEE Trans. Biomed. Circuits Syst.*, vol. 14, no. 6, pp. 1160–1178, Dec. 2020. doi: 10.1109/TBCAS.2020.3038599

[9] M.-J. Liu and S. S. H. Hsu, "A Miniature 300-MHz Resonant DC–DC Converter With GaN and CMOS Integrated in IPD Technology," *IEEE Trans. Power Electron.*, vol. 33, no. 11, pp. 9656–9668, Nov. 2018. doi: 10.1109/TPEL.2017.2788946

[10] I. A. Mashhadi, M. Pahlevani, S. Hor, H. Pahlevani, and E. Adib, "A New Wireless Power-Transfer Circuit for Retinal Prosthesis," *IEEE Trans. Power Electron.*, vol. 34, no. 7, pp. 6425–6439, Jul. 2019. doi: 10.1109/TPEL.2018.2872844

[11] T. Nagashima *et al.*, "Steady-state analysis of isolated class-e^2 converter outside nominal operation," *IEEE Trans. Ind. Electron*, vol. 64, no. 4, pp. 3227–3238, Apr. 2017. doi: 10.1109/TIE.2016.2631439

[12] T. Nagashima, X. Wei, E. Bou, E. Alarcon, and H. Sekiya, "Analytical design for resonant inductive coupling wireless power transfer system with class-E inverter and class-DE rectifier," in *2015 IEEE International Symposium on Circuits and Systems (ISCAS)*. Lisbon, Portugal: IEEE, May 2015, pp. 686–689. doi: 10.1109/ISCAS.2015.7168726

[13] A. Celentano *et al.*, "A Primary-side Maximum Efficiency Transfer Solution in Wireless Power Transfer Systems: Theory and Validation," *TechRxiv Preprint*, 2023.

[14] Y. Liu and H. Feng, "Maximum Efficiency Tracking Control Method for WPT System Based on Dynamic Coupling Coefficient Identification and Impedance Matching Network," *IEEE J. Emerg. Sel. Topics Power Electron.*, vol. 8, no. 4, pp. 3633–3643, Dec. 2020. doi: 10.1109/JESTPE.2019.2935219

[15] M. Ghovanloo and S. Atluri, "An Integrated Full-Wave CMOS Rectifier With Built-In Back Telemetry for RFID and Implantable Biomedical Applications," *IEEE Trans. Circuits Syst. I, Reg. Papers*, vol. 55, no. 10, pp. 3328–3334, Nov. 2008. doi: 10.1109/TCSI.2008.924877

[16] M. Kiani and M. Ghovanloo, "An RFID-Based Closed-Loop Wireless Power Transmission System for Biomedical Applications," *IEEE Trans. Circuits Syst. II Express Briefs*, vol. 57, no. 4, pp. 260–264, Apr. 2010. doi: 10.1109/TCSII.2010.2043470

[17] A. Celentano *et al.*, "A Wireless Power Transfer System for Biomedical Implants based on an isolated Class-E DC-DC Converter with Power Regulation Capability," in *63rd Intern. Midwest Symp. on Circ. and Systems*, Aug. 2020, pp. 190–193. doi: 10.1109/MWSCAS48704.2020.9184689